High power electromagnetic vibration harvesting using a magnetic dumbbell structure

Holm, P.; Imbaquingo, C.; Mann, B.P.; Bjørk, R.

Published in:
Journal of Sound and Vibration

Link to article, DOI:
10.1016/j.jsv.2022.117446

Publication date:
2023

Document Version
Publisher's PDF, also known as Version of record

Journal of Sound and Vibration 546 (2023) 117446

Contents lists available at ScienceDirect

Journal of Sound and Vibration

journal homepage: www.elsevier.com/locate/jsvi

High power electromagnetic vibration harvesting using a magnetic dumbbell structure

P. Holm [a], C. Imbaquingo [a], B.P. Mann [b], R. Bjørk [a,*]

[a] Department of Energy Conversion and Storage, Technical University of Denmark - DTU, Anker Engelunds Vej 1, DK-2800 Kgs. Lyngby, Denmark

[b] Department of Mechanical Engineering and Materials Science, Duke University, Durham, NC 27708, USA

ARTICLE INFO

Keywords:
Electromagnetic vibration energy harvester
Vibration
Harvesting
Electromagnetism
Soft resonator
Softening response

ABSTRACT

This paper considers an electromagnetic energy harvester consisting of a tube with two fixed magnets and two coils and containing a floating free-to-move dumbbell structure with two magnets. The dumbbell shape has a number of benefits, including an increased changing magnetic flux, a controllable resonance frequency and reduced friction. We experimentally characterize the power produced by the harvester between 4 Hz and 20 Hz in steps of 0.5 Hz for a fixed excitation amplitude of 3 mm. The frequency is swept in both ascending and descending order. The maximum power produced by the harvester is 1.04 mW which occurs at 8.5 Hz in descending frequency sweep where the maximum acceleration of the harvester is 0.87 g. The power density of the harvester is 50 μW/cm^3 and the power per unit mass is 32 μW/g. The dumbbell harvester shows a softening resonator response with hysteresis between ascending and descending frequency sweeps. Furthermore, the harvester has two resonance peaks in power as a function of the drive frequency, with the peaks being of almost equal magnitude. Finally, a Fourier analysis shows the two resonance peaks have different harmonics, with the first resonance peak being characterized by higher-order harmonics whereas the second resonance peak is characterized by a response at the excitation frequency.

1. Introduction

Powering sensors, wearable and Internet-of-Things (IoT) devices will require a tremendous amount of energy in the near future [1–3]. Currently, these devices are powered by batteries, but this is far from an ideal situation, as batteries have to be changed every couple of years which, given the number of IoT-devices projected in the near future, will be a monumental task. Furthermore, battery production can pollute the environment.

In recent years, energy harvesting directly from the environment has been considered to be a promising power source for sensors and IoT-devices. Numerous harvesting techniques exists, adapted to different environmental sources. The most abundant of these ambient sources of energy is vibrations, which are present in both indoor and outdoor environments, and available throughout the day.

There are two primary ways of converting vibrational energy into electrical energy, i.e. using either the piezoelectric effect or electromagnetic energy conversion. This paper considers a specific case of the latter. In an electromagnetic harvester (EMVEH), a permanent magnet is displaced relative to one or more coils, thereby inducing a voltage across the coil(s) according to Faraday's law. The archetypical EMVEH [4] consists of two fixed magnets placed at either end of a tube with a free magnet inside the tube between

* Corresponding author.
E-mail address: rabj@dtu.dk (R. Bjørk).

https://doi.org/10.1016/j.jsv.2022.117446
Received 7 July 2022; Received in revised form 8 November 2022; Accepted 13 November 2022
Available online 17 November 2022

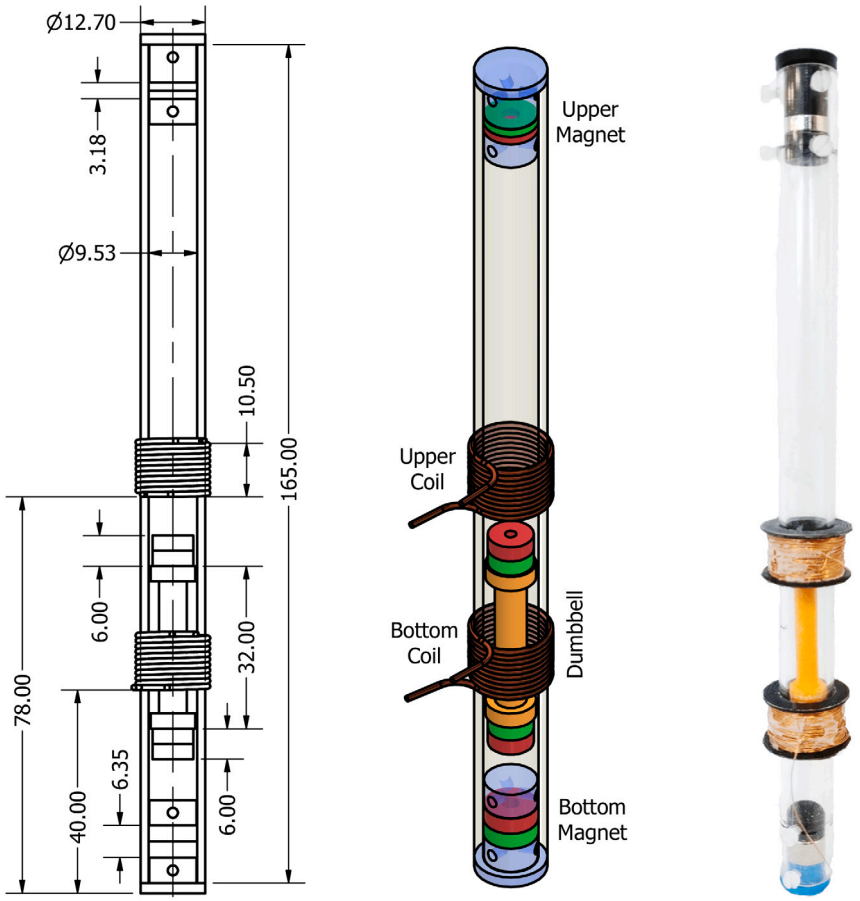

Fig. 1. The dumbbell harvester is shown as a technical drawing (left), schematic illustration (middle), and an actual photo of the harvester (right). The polarity of the magnets is indicated by the red/green color. On the right, the dumbbell is partly obscured by the coils. The dimensions of the harvester can be found in Table 1. (For interpretation of the references to color in this figure legend, the reader is referred to the web version of this article.)

these. The free magnet has an opposite polarity compared to the fixed magnets, causing this to be repelled by both fixed magnets, making it float inside the tube. Surrounding the tube at selected positions are one or more coils, through which the floating magnet will then pass when the EMVEH is vibrated. Two-dimensional versions of EMVEHs, which has a more easily tuneable bandwidth and can harvest vibrations in two dimensions also exist [5–7]. The typical applications for EMVEHs are energy extraction from human motion to power sensors [8–15], but other niche applications, such as EMVEHs for ocean wave energy harvesting, have also been demonstrated [16]. Other EMVEH designs, such as pendulums [17], swinging ring designs [18], slotted disc springs [19] or roly-poly-like motion [20] have also been studied.

There are two outstanding issues with EMVEHs that limit their applicability, namely their small frequency bandwidth and their internal friction. Regarding the former, EMVEHs have been studied extensively in recent years and numerous prototypes with varying number of magnets have been tested; see Ref. [21] for a recent review of the field. Most EMVEHs display a single resonance peak in generated power as function of drive frequency [4,16,22–27] which makes the usable frequency bandwidth at which the harvester can produce power narrow. While a few select harvesters do have multiple peaks in their generated power as function of drive frequency [28,29], the secondary peaks are much lower in power than the resonance peak. To circumvent the narrow frequency span of EMVEHs efforts to make a self-adaptive EMVEH by changing its effective length and thus resonance frequency has recently been demonstrated [23], with a gain in output power of around 30%. However, a wider frequency bandwidth would be a simpler and thus preferable solution.

Regarding the issue of internal friction in the EMVEH, it is the case with all EMVEHs that there is friction between the floating magnet and the walls of the confining tube. This friction has long been acknowledged to be a problem in these designs [4] and it has a significant impact on the power production of the harvester [30] with the produced voltage in some cases being a factor of five times lower than in the case of zero friction [31].

This paper presents a new EMVEH design with lower internal friction, that at the same time displays previously unseen power characteristics, both in terms of resonator behavior and frequency response. The harvester has a broader and potentially more easily tunable frequency bandwidth than existing harvesters. This work is structured as follows. First, this new dumbbell

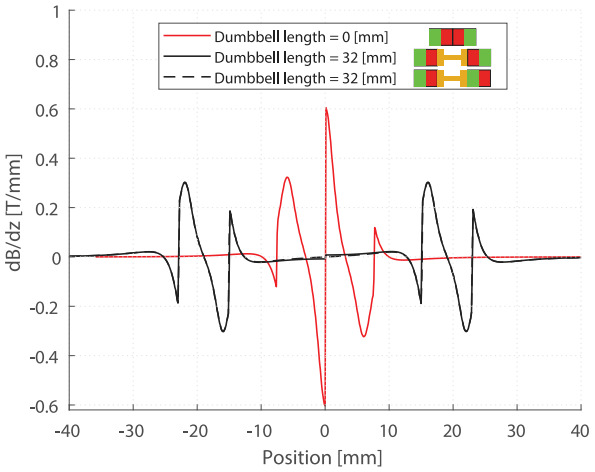

Fig. 2. The gradient of the magnetic flux density as computed using Comsol for the dumbbell dimensions given in Table 1 along the center of the tube for three different magnet configurations. The color in the legend indicate the poles on the magnets. (For interpretation of the references to color in this figure legend, the reader is referred to the web version of this article.)

electromagnetic energy harvester is presented. The dimensions of the harvester are provided along with some considerations for the chosen parameters. Following this, the experimental procedure for testing the harvester is described and the experimental results are presented. Here the focus is on the frequency response, i.e. the power produced as function of the excitation or drive frequency, for the harvester and its hysteresis properties. The voltage produced by the harvester is broken down into frequency components and these are analyzed in detail as a function of the drive frequency. Finally, the performance of the harvester is compared to other published harvesters before the concluding remarks.

2. The dumbbell harvester

In conventional EMVEHs harvesting applications, vibrations are harvested in one dimension and a free magnet is constrained to move along a single axis through one or more coils, thereby inducing an electromotive force. The free magnet is levitated between two fixed magnets with opposite polarities in order to reduce friction in the system. However, as Earnshaws theorem states, the levitation is unstable and the free magnet must be confined in a tube to prevent it from flipping over. This, however, can result in significant friction between the free magnet and the tube. To overcome this friction, we consider a design where the conventional free magnet is replaced by a dumbbell structure where two magnets are attached together with a plastic connector piece. The dumbbell EMVEH is illustrated in Fig. 1 . EMVEH designs with multiple floating magnets are known from literature [15,21,32], e.g. a design with five floating magnets and three coils [31], but here the spacers between the magnets are of a similar shape as the free cylindrical magnets, thus they still contribute significant friction in the design. This is also seen in other designs with multiple free magnets [33].

There are several benefits to using a dumbbell structure. Compared to a magnet of similar length, the area of the dumbbell in contact with the walls of the tube is much lower, reducing the internal friction in the harvester. However, there are additional benefits to the dumbbell system. First of all, compared to a conventional EMVEH with one large magnet and no dumbbell, the dumbbells length can be tuned, thereby changing the resonance frequency of the system. This can be seen from the fact that a longer dumbbell floating magnet will have to travel a shorter distance before having traversed the length of the tube. Thus the length of the dumbbell can be used to tune the resonance frequency of the harvester. Secondly, in a system with two coils, at any given moment there is a magnet moving through each coil. Finally, and most importantly, the magnets in the dumbbell can be arranged in polarity in a way that brings about an additional magnetic flux minima between the two magnets in the dumbbell. By placing the magnets in the dumbbell with opposite polarity the magnetic flux density has to be zero at the middle of the dumbbell, which results in an increased voltage induced in the coils when the dumbbell passes through the coils, i.e. an increased amount in comparison to a dumbbell with aligned polarity. This can be seen from Fig. 2, which shows the change in magnetic flux density for the dumbbell structure throughout the length of the tube. If the dumbbell had not been present, i.e. two magnets with opposite polarity had simply been glued together, there would be two fewer magnetic flux density minima. The area enclosed by each curve in Fig. 2 is a direct measure of how much voltage can be induced in a coil by the dumbbell structure. For the case of no dumbbell structure, the absolute area beneath the curve is 3.88 T, while for the case of the dumbbell with opposite polarity the area is 4.10 T. Finally for the case of the dumbbell with similar polarity the area is 4.02 T. Thus it is clear that the dumbbell structure with opposite polarity, as is studied in this work, can induce a higher voltage in a coil, compared to a regular floating magnet.

All magnets used in the dumbbell design are cylindrical in shape. As it is desirable that the harvester be as light as possible, such that the energy from vibrations be maximally utilized, hollow cylindrical magnets are used. Furthermore, almost all EMVEH harvesters operate in an orientation parallel to gravity. In the design presented here, we therefore increase the size of the bottom

Table 1
Dimensions of the components of the harvester. "Common" refers to a parameter shared between two components, e.g. both coils having the same height. Position is measured from the bottom end of the harvester. Note that there are two identical free magnets on the dumbbell. The harvester has a mass of 32.5 g.

Component		Parameter	Quantity
Fixed magnet(s)	*Common*	Inner diameter	3.175 mm
		Outer diameter	9.525 mm
		Magnetization	1.32–1.37 T
	Bottom	Height	6.35 mm
	Top	Height	3.175 mm
Free magnet(s)		Inner diameter	2.0 mm
		Outer diameter	8.0 mm
		Height	6.0 mm
		Mass	3.0 g
		Magnetization	1.40–1.46 T
Tube		Inner diameter	9.525 mm
		Outer diameter	12.7 mm
		Length	165 mm
		Dumbbell length	32 mm
Coil(s)	*Common*	Height	12 mm
		Gauge	0.2 mm
		Turns	200
	Lower	Position	40 mm
		Resistance	6.1 Ω
		Inductance	551 μH
	Upper	Position	78 mm
		Resistance	5.4 Ω
		Inductance	450 μH

fixed magnet, to compensate for the gravitational force. Conversely, the top magnet is smaller since it only needs to repel the upward movement of the dumbbell. Such a design with an asymmetric configuration of fixed magnets is also uncommon. Typically, EMVEHs designs use a symmetric agreement of fixed magnets, i.e. with the same top and bottom magnet, but designs exists with only a single magnet at the bottom, i.e. no top magnet [15]. Finally, as gravity will displace the equilibrium position of the dumbbell from the center of the tube, the coils are not placed symmetrically with respect to the tube center, but instead with respect to the equilibrium position of the dumbbell in gravity.

To characterize the performance of a dumbbell EMVEH, a specific harvester has been produced. The dimensions of this harvester, i.e. magnets, coils etc., as well as other relevant parameters, can be found in Table 1. The coil resistance and inductance was measured at 1 KHz using a Keysight U1732C LCR meter.

3. Experimental setup

The dumbbell electromagnetic vibrational energy harvester must be characterized in terms of the power it produces as function of frequency of the vibrational source to which it is attached to evaluate its usefulness. In this work we use a completely standardized, lab-based and most importantly repeatable, way of testing and characterizing the performance of the proposed harvester.

The experimental setup for the harvester characterization is shown in Fig. 3 and consists of a mechanical and electrical part. Mechanically, a sinusoidal vibration of a specified amplitude and frequency was applied to the harvester using a Dewesoft DS-PM-250 SN A-21-00221 shaker. The amplitude of vibration was regulated by a PID-controller and the frequency was varied in the experiment from 4 Hz to 20 Hz. The prototype was elevated from the structure such that it did not couple to the magnetic field intrinsic to the shaker. For all experiments, the amplitude of the vibrating source was held constant at 3 mm, i.e. 6 mm peak-to-peak.

The frequency range of these experiments was only slightly larger than the dominant step frequency of human walking, which is centered around 2–3 Hz [34], and most wearable energy harvesters have a resonant frequency matching one of the higher harmonics of the walking frequency range [34]. In fact, harvesting energy from human motion has been a key focus of EMVEH development [8–15]. However, we note that the harvester presented here is by no means limited to wearable applications, but can be used to harvest power for any vibrational source within its frequency range.

Regarding the electrical setup, the two coils in the harvester are connected in series across a load resistance equal to the sum of the internal resistances of the two coils, 11.5 Ω, in accordance with the Maximum Power Transfer Theorem [35]. This voltage signal was then measured differentially using a National Instruments USB-6351 DAQ, using a sampling frequency of $f_s = 5$ KHz. The sampling frequency was chosen in accordance with the Nyquist Theorem, such that it far exceeded twice the highest frequency component of the measured signal. Since the harvester is a floating signal source, two resistors are added to provide return paths for bias current and avoid measurement error. The resistors were chosen to be large (47 kΩ) to reduce the parasitic effect of these,

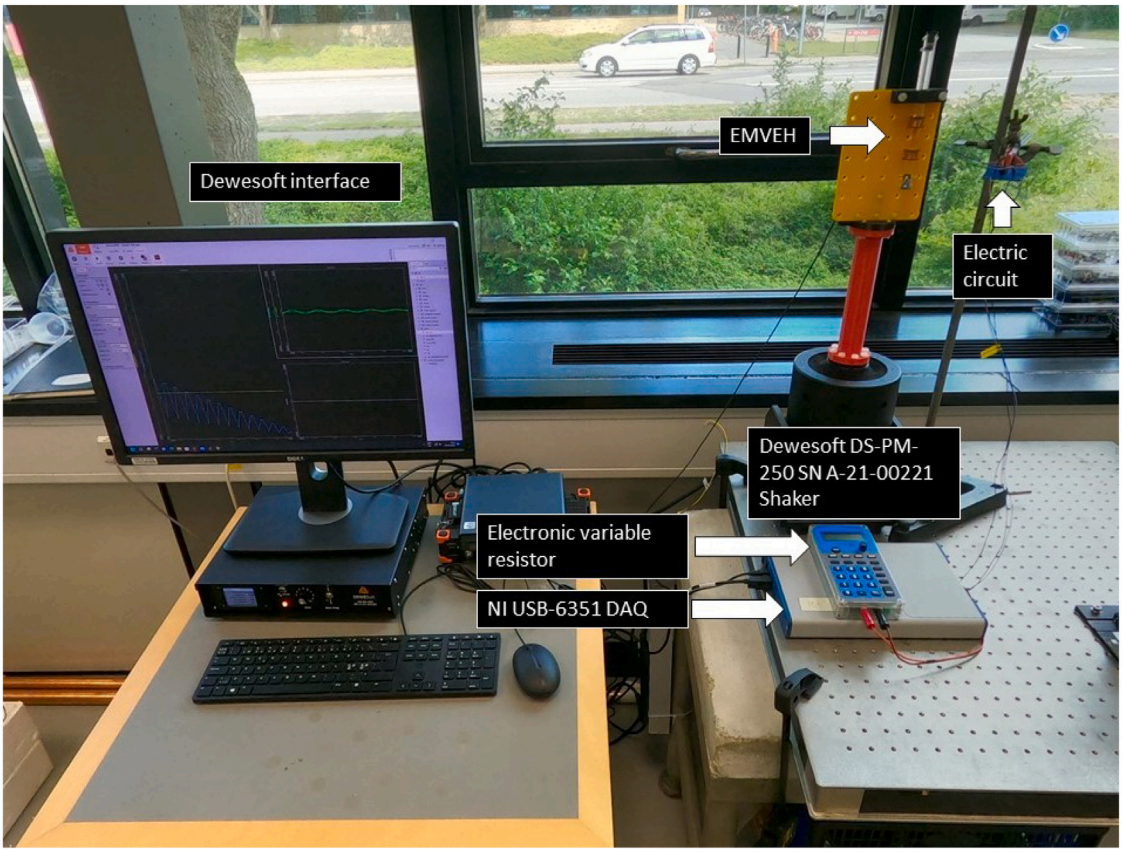

Fig. 3. Experimental setup where the harvester is mounted onto a Dewesoft DS-PM-250 SN A-21-00221 and the resulting voltage signal is measured using a NI DAQ.

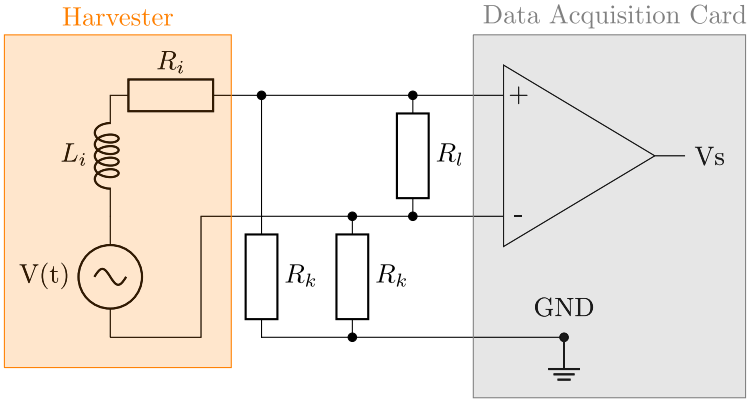

Fig. 4. Equivalent electrical circuit model of the EMVEH. R_i and L_i are the internal resistance and inductance of the two coils, respectively. R_k are resistors added to avoid floating point measurement errors, and R_l is the load resistance across which voltage is measured.

thus the measured voltage is only slightly less than the maximum potential value. The electrical circuit of the system is shown in Fig. 4.

The electrical characterization of the harvester is done when the system, for a specific frequency, has reached steady state. This is ensured by investigating the measured voltage waveform, for which the waveform should be periodically constant with time. Typically, the steady state is reached within seconds at a given drive frequency. Once the voltage signal has reached steady state, the voltage is recorded for 10 s to allow for sufficient periods to reliably calculate the RMS voltage, V_{rms}. Since the signal is connected

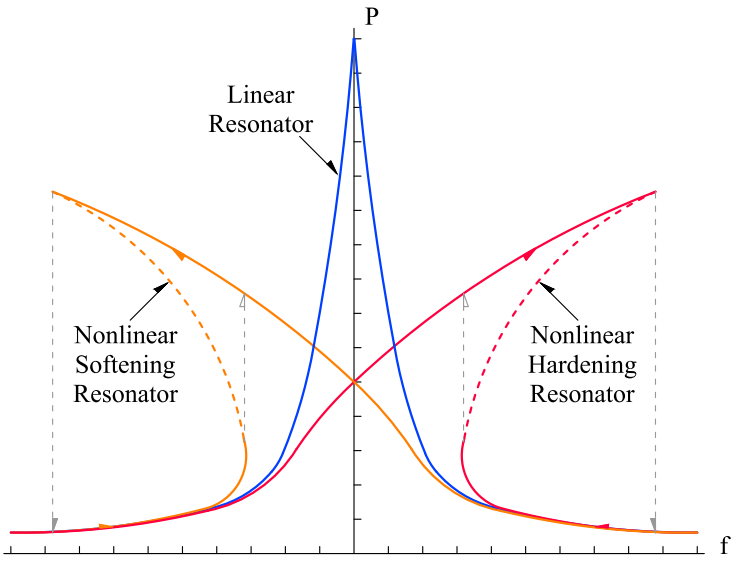

Fig. 5. The power produced as function of frequency for both linear and nonlinear frequency responses [9]. The arrows indicate the direction that the frequency is changed in.

across a load resistance, the power can then be found by Eq. (1)

$$P = \frac{V_{\text{rms}}^2}{R_l} \tag{1}$$

where R_l is the load resistance. This output energy of the harvester is the power directly usable by any e.g. IoT device connected to the harvester.

4. Harvester frequency response

The power that can be harvester from an EMVEH depends on the frequency of the vibration source. Therefore, EMVEHs are always characterized by the power they produce as function of drive frequency, i.e. their frequency response is measured [4,22,23,36]. The simplest possible EMVEH which consists of a magnet attached to a mechanical spring will generally presents a linear frequency response as shown in Fig. 5, due to the linear spring force. However, in most EMVEHs the restoring force is provided by non-linear magnetic repulsion. This changes the frequency response to a nonlinear resonator behavior. Depending on the nonlinear characteristics, the resonator can present a hardening or softening effect, where the former is characterized by the effective resonance frequency increasing with the amplitude of external vibrations, and vice versa for the latter. The frequency response also shows hysteresis, with a hard resonator having an increased power with increasing frequency compared to decreasing frequency and vice versa for a soft resonator [37], as illustrated in Fig. 5.

Here, we characterized the designed dumbbell EMVEH by performing a sweep in drive frequency from 4 to 20 Hz in steps of 0.5 Hz in both increasing and decreasing frequency sweeps. The lower bound is chosen because below this frequency there is very little movement of the floating dumbbell structure and the upper bound chosen to avoid mechanical catastrophe. The frequency is changed manually in steps of 0.5 Hz such that it can be verified that the system has settled into steady state. As an example, Fig. 6 shows the voltage as function for time for a 1 s interval for a frequency of 7.5 Hz, for the case where frequency has been increased from 4 Hz.

As stated above, the drive frequency was swept in either ascending order or descending order, i.e. either from 4 Hz to 20 Hz or vice versa. This was done to investigate the presence of hysteresis, i.e. the pathway dependence of the resulting voltage, which is known to be present in EMVEHs [4,22,23,36]. The power as calculated using Eq. (1) as function of drive frequency for increasing and decreasing frequency sweeps, termed ascending and descending respectively, is shown in Fig. 7. As can be seen from the figure the harvester shows a clear resonance behavior with the first resonance peak at around 5 Hz and the following peak at around 10 Hz for the ascending sweep. The reason that the system displays two peaks will be discussed subsequently. The first resonance peak, which is smaller in power, appears at about half the frequency of the larger resonance peak, as will also be discussed subsequently. Two such resonance peaks are often termed the subharmonic resonance and primary resonance peaks. We note that the ascending and descending experiments were done separately of each other, stopping the shaker in between the experiments. Thus the fact that the same power is obtained at high frequency is a testament to the repeatability of the measurements.

The harvester shows a clear hysteresis behavior in the region from 8 to 10 Hz, with the descending power being up to 10 times higher than the ascending power at the same frequency within this range of drive frequencies. The hysteresis region, which has also

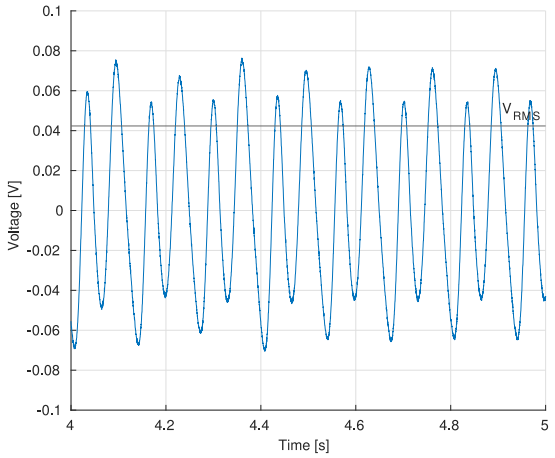

Fig. 6. A 1 s interval of the voltage waveform at a drive frequency of 7.5 Hz in ascending sweep.

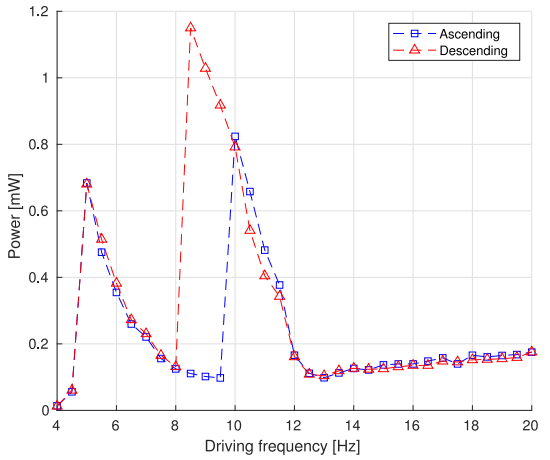

Fig. 7. Power with respect to drive frequency for at frequency sweep in both ascending and descending frequency.

been observed in other EMVEH harvesters [4,22,23,36], clearly shows that multiple stable solutions exists in the harvester phase space [23,29,38,39]. The maximum power was obtained for a descending frequency sweep near 8.5 Hz where a power of 1.04 mW was obtained. We note that the coils chosen for this setup were not optimized in any way, i.e. a larger power could undoubtedly be produced by increasing the size of the coils. However, the goal of the investigation presented here was to explore the frequency behavior caused by the dumbbell structure as opposed to producing the largest power possible.

4.1. Resonator behavior

It is of interest to compare the response of the present harvester against those described in the literature, e.g. Ref. [21] as well as additional newer references. The overwhelming majority of these describe an EMVEH that displays a single resonance peak as function of frequency with a clear hardening behavior [4,16,22–26,40]. This is also the case for numerical models of EMVEHs, where the same single peak hardening behavior is observed [36]. Experimental EMVEHs with multiple magnets, somewhat like the EMVEH described in this work, also display a nonlinear hardening resonator behavior with a single peak [27], even though up to six floating magnets are used [14].

There are a few cases that deviate from the standard nonlinear hardening resonator, single peak EMVEH. The harvester tested in Ref. [29] also has a nonlinear hardening resonator behavior, but this displays multiple peaks in power as function of frequency. However, there the higher frequency peaks are lower in power than the low frequency peaks, opposite of what is observed in this work. Their second peak as function of frequency is also only observable in one frequency direction, i.e. not both ascending and descending mode. In Ref. [28] a nonlinear hardening resonator behavior is also seen, with a peak at a frequency half of the resonance peak. However, this peak is an order of magnitude lower in V_{rms} than the main resonance peak.

Regarding softening resonator behavior, only two studies have reported this behavior. The harvester in Ref. [38] display an extremely small nonlinear softening resonator peak at very low frequencies but it is much smaller than the peak observed here.

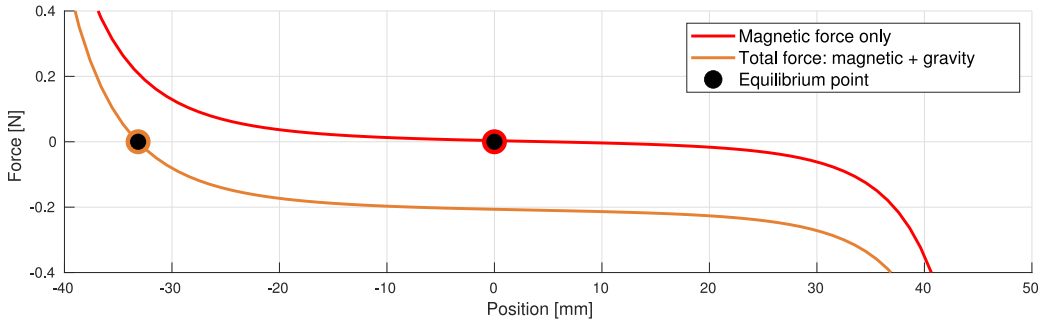

Fig. 8. Force as a function of position for linear and nonlinear resonators as calculated using the verified analytical expression from Ref. [41] for the dumbbell dimensions given in Table 1.

Finally, Ref. [31] reports seeing a softening response, but only reports a single peak in power as function of frequency. Furthermore, the EMVEH tested in that work has five free magnets and three coils, so it is significantly more complicated than the EMVEH presented here.

Clearly, the dumbbell harvester studied here has a nonlinear softening resonator behavior, which is novel for EMVEHs. We hypothesize that this particular frequency response comes from the magnetic restoring force inherent in the harvester. In Fig. 8 we show the magnetic restoring force on the dumbbell as calculated using the verified analytical expression from Ref. [41], and as can be seen when the gravitational force in included the equilibrium point of the nonlinear force curve is 30 mm below the center of the harvester housing. This results in three distinct stages that the dumbbell experiences when the harvester is vibrating. The first stage occurs around the dumbbell equilibrium point of Fig. 8, where the magnetic resulting force between the dumbbell and the bottom magnet varies nonlinearly. The second stage is the middle linear portion of the force curve. If the dumbbell only moves between these two stages, the first resonance peak shows up. However, when the input frequency increases, the dumbbell reaches the third stage in the top of the tube where the dumbbell interacts with the top magnet, and thus the resulting force again becomes nonlinear. This creates the two peaks in the resonance response shown in Fig. 7. Thus the two resonance peaks observed here are caused by the long length of the tube, allowing the harvester to either experience two or three stages. In addition, the nonlinear softening resonator behavior results from letting the force of gravity play a role in the system, unlike Ref. [40] where the magnetic restoring force was so strong that the gravity force could not influence the harvester behavior and hence the second stage was almost neglected.

4.2. Coil damping

The hysteresis region of the EMVEH is a result of the non-linearity of the EMVEH, i.e. there are multiple stable solutions at a given drive frequency. A linear system would settle into a unique steady-state regardless of the initial conditions of the EMVEH. The non-linearity of the EMVEH comes from multiple effects; the magnetic restoring force which is a non-linear function of distance and the damping from the coils which depends upon the velocity of the dumbbell. The damping of the coils is a consequence of Lenz's law.

In order to determine the role of the latter on the observed hysteresis properties the frequency sweep experiment described above was repeated but with the load resistance replaced by an open-circuit. This means that no current flows in the coils and thus there is no resulting damping. Since there is no load resistance attached ($R = \infty$), the EMVEH generates no power. Instead the results are represented by the RMS voltage. The comparison of the results for the matched load, i.e. the results shown in Fig. 7 except displayed in terms of V_{rms}, and the open-circuit experiments are shown in Fig. 9.

As can be seen in Fig. 9(b), hysteresis is still clearly present in the harvester when using an open circuit. Therefore the hysteresis behavior is attributable to the non-linear restoring force of the magnets and not to the coils. However, the nonlinearity of the magnet–coil interaction can create a different outcome if bigger coil windings are considered. Additionally, it should be noted that the friction from the movement of the dumbbell against the tube is also a source of non-linearity, however this is assumed to be negligible. Note that the first resonance peak shifts by 0.5 Hz towards lower frequency for the case of open circuit compared to matched resistance, while the second resonance peak is unaffected by the change in resistance.

To explore the similarity in the RMS voltage for the case of matched resistance and open circuit, we in Fig. 10 show the voltage as function of time, i.e. the voltage waveform, at resonance for these two cases. As can be seen from the figure, the voltage signals are very alike as function of time, with the open circuit voltage obviously being higher than the match resistance voltage.

4.3. Waveform characterization

As discussed above, the response of the EMVEH is highly non-linear with respect to the drive frequency, f_d. Previously, the steady-state response at each drive frequency was summarized by either the RMS voltage or power. In the following a deeper investigation into how the shape of the waveform changes across a frequency sweep is conducted.

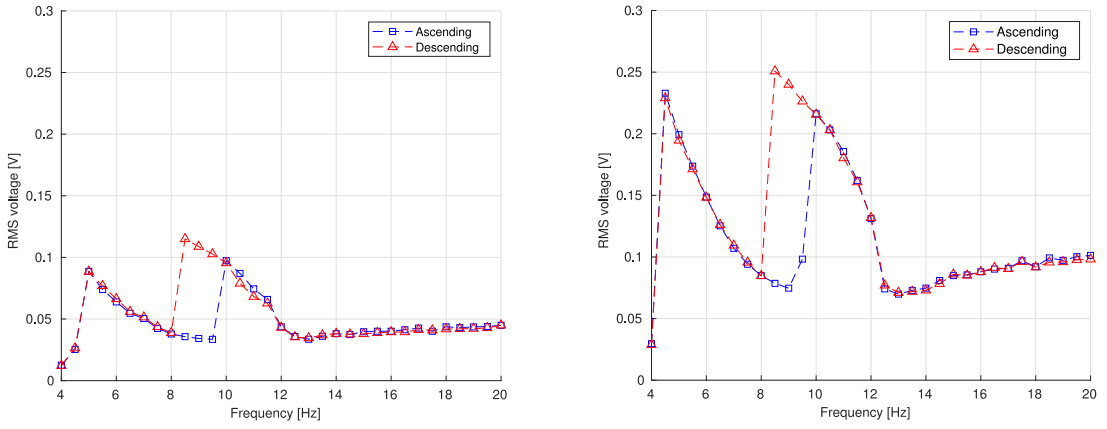

(a) Matched resistance ($R_L = 11.5\Omega$). (b) Open circuit.

Fig. 9. V_{rms} as function of frequency for (a) the matched resistance case, and (b), the open circuit case, for both ascending and descending frequency.

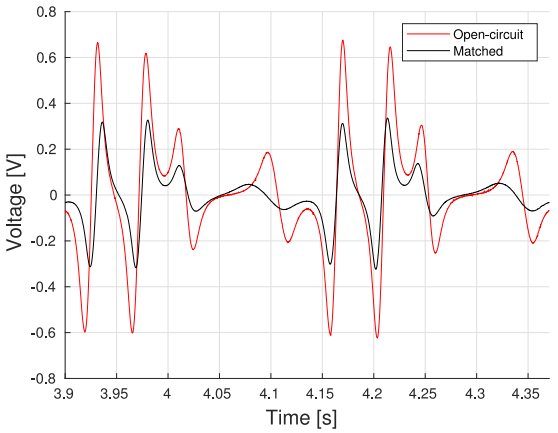

Fig. 10. Output voltage for the descending sweep at $f_d = 8.5$ Hz for both matched load and open-circuit.

We performed a Fourier spectral analysis where the voltage signal was represented by its spectral amplitude components. The voltage signals are periodic and thus the Fourier spectrum will consist of a set of harmonics located at integer multiples of some fundamental frequency. It is of particular interest how the various harmonics of the signal compare to the specific drive frequency of the signal. The voltage signals are sampled and are therefore discrete. Therefore, a discrete Fourier Transform is needed. Matlab's Fast Fourier Transform (FFT) is used to this end, the definition of which is seen in Eq. (2).

$$F(k) = \sum_{j=1}^{n} V(j) W_n^{(j-1)(k-1)} \qquad \text{with} \qquad W_n = \mathrm{e}^{-2\pi i/n} \tag{2}$$

where e is Euler's number and $V(j)$ is the voltage signal. The Fourier transform of the signal is represented by the norm-square, $|F(k)|^2$, and the phase is disregarded. In this way, an overview of the main harmonics of the signal can be obtained. The frequency resolution in the Fourier-domain is effectively dictated by how many periods of the signal that are sampled. The signal is sampled for $T = 10$ s at a sampling frequency of $f_s = 5$ kHz for a total of $N = T \cdot f_s = 10000$ samples. As seen in Fig. 6, a period lasts roughly 0.1 s. Therefore, plenty of periods are sampled to obtain a sufficient frequency resolution. Quantitatively, the resolution is given by $\Delta f = \frac{f_s}{N} = \frac{f_s}{T \cdot f_s} = \frac{1}{T} = 0.1$, which dictates the minimum spacing between points of the Fourier transform.

An example of the Fourier analysis is shown for a drive frequency of $f_d = 10$ Hz in Fig. 11. First, the voltage signal is considered in the time-domain in Fig. 11(a). Next, the norm-square of the Fourier transform is computed, using the FFT. Since the signal is real, the norm-square is symmetric. As a result only a single-sided spectrum need be considered, where the Fourier transform is scaled by 2. The signal is not normalized with respect to the number of samples since there is no intention to transform back to the time-domain. The specific size of the norm-square is not of interest, only the relative sizes compared to the other harmonics of the Fourier spectrum. The frequency axis in the Fourier domain, k, is normalized with respect to the drive frequency, f_d, such that the normalized frequency axis is $k_d = \frac{k}{f_d}$. This is because how the harmonics relate to the drive frequency is of particular interest

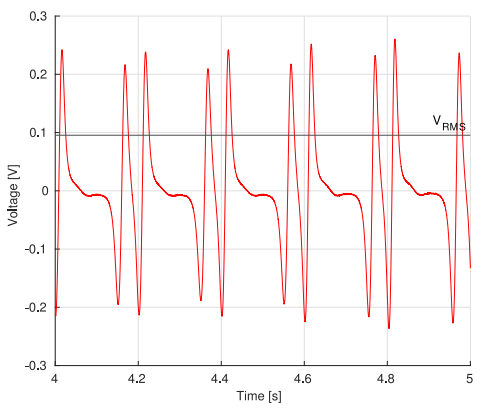

(a) Time-domain representation.

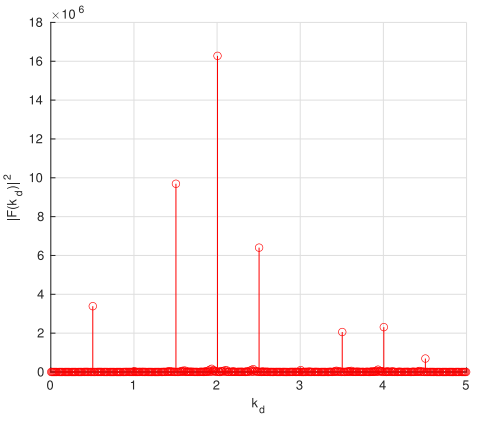

(b) Fourier-domain representation.

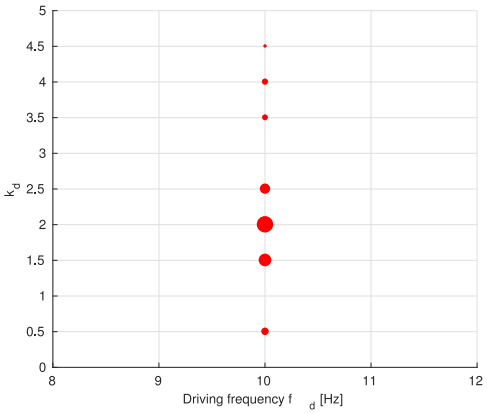

(c) Fourier-domain composition where marker size is proportional to $|F(k_d)|^2$.

Fig. 11. A representative one-second segment of the voltage response for the descending sweep for $f_d = 10$ Hz in the (a) time-domain and (b) Fourier-domain. (c) Representation of the Fourier-domain where the marker size is proportional to the norm-square of the Fourier harmonic.

physically. As can be seen in Fig. 11(b), the harmonics occur at integer or half-integer multiples of the drive frequency. As will be seen, this pattern is not unique to this waveform.

To visualize the Fourier composition at all frequencies of the ascending and descending frequency sweep, we show the norm-square of the Fourier-transform graphically in Fig. 11(c). The normalized Fourier frequency axis, k_d, is now shown on the vertical axis, and the drive frequency is shown on the horizontal axis as in Fig. 7. Finally, the norm-square of the Fourier transform is represented by the size of the marker, for which the area of the marker circle was chosen to be proportional to the norm-square. In order to sort out noise and only identify significant peaks a peak prominence of $|F(k_d)|^2 \geq 0.2 \cdot 10^6$ is specified.

This aforementioned process was repeated for all the signals in both the frequency sweeps and the results are shown in Fig. 12. The results reveal interesting results about the dynamics of the EMVEH's response through the frequency sweep. Clearly, the pattern of the harmonics being located at integer-or half-integer multiples of the drive frequency occurs throughout frequency space. Many of the signals have a significant component at twice the drive frequency. This was because a single motion of one of the magnet in the dumbbell through a coil (back and forth) results in two voltage periods. This was the dominant feature in the upper frequency range, i.e. after the 2nd resonance peak, where the voltage waveform is characterized by a simple Fourier composition. In this region, the power was approximately a linear function of the drive frequency as seen in Fig. 7.

The Fourier composition changes dramatically near resonance. The resonant peaks, where the second is located at a different drive frequency for the ascending and descending sweep respectively, are indicated by lines in Fig. 12. Around this region there is an appearance of multiple harmonics revealing a richer response. We note that the Fourier composition is reflected in the behavior of power as function of frequency. In the ascending sweep, Fig. 12(a), the harmonics appear suddenly in the same way that the resonance appears suddenly in Fig. 7. Conversely, the harmonics appear gradually in the descending sweeps just like how the power gradually increases in Fig. 7. It is also of significant interest that the main frequencies changes significantly between the two resonance peaks, with the first resonance peak clearly being dominated by larger-order harmonics compared to the second resonance peak.

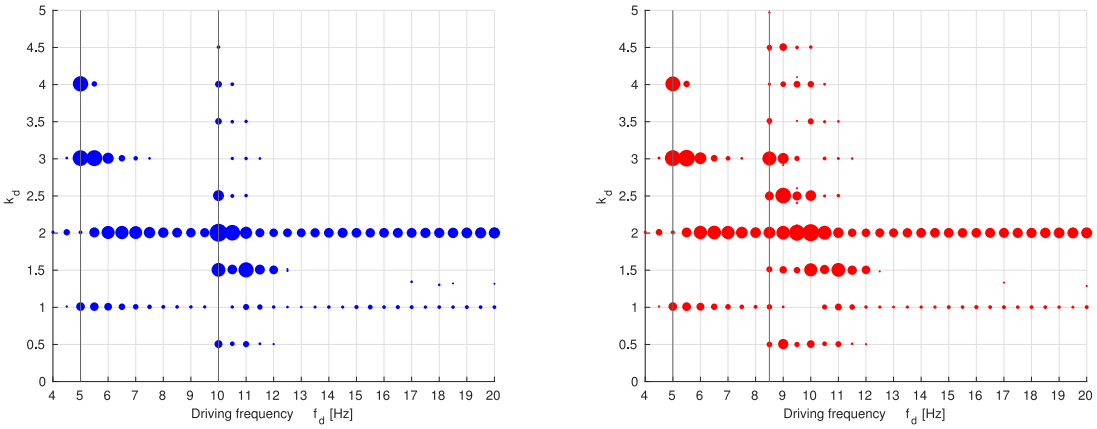

(a) Fourier composition for ascending.

(b) Fourier composition for descending.

Fig. 12. The Fourier spectrum of the (a) ascending and (b) descending frequency sweeps. The first and second resonant peaks are marked by a line for each sweep and the radius of each marker is proportional to the norm-squared of the Fourier Transform.

Table 2
A comparison of the performance characteristics of the dumbbell harvester presented in this work to similar EMVEH harvesters where details on either the total mass or total volume of the system could be found.

Reference	Mass	Acc.	Freq.	Power	Power density pr.		Notes
					vol.	mass	
	[g]	[m/s^2]	[Hz]	[μW]	[μW/cm^3]	[μW/g]	
This work	32.5	0.87 g	8.5	1040	50	32	
Liu (2014) [10]	–	0.54 g	4.5	284	45.3	–	
Berdy (2015) [12]	–	0.1 g	6.7	410	34.2	–	
Geisler (2017) [13]	–	2g	6	6570	730	–	5 × 2800 turns
Struwig (2018) [15]	31.5	2.2 g	2.2	3010	179	95.5	910 turns [21]
Nammari (2018) [42]	–	1g	15.5	~ 6000	132.25		Magnet mass 13 g
Wang (2017) [14]	218.7	0.85 g	9.2	10600	–	48.5	480 turns

5. Discussion

It is clearly of interest to compare the performance of the presented EMVEH to similar harvesters in literature. As mentioned previously, the maximum power produced by the harvester is 1.04 mW which occurs at 8.5 Hz in the descending frequency sweep. Given the overall cylindrical shape of the harvester with the dimensions given in Table 1, the power density is calculated to be 50 μW/cm^3. The maximum acceleration of the harvester at the drive frequency of 8.5 Hz, which is where maximum power can be harvested, is $a_z = 0.87$g. Compared to similar harvesters, as tabulated in Ref. [21], this is a reasonable power density, especially considering the fact that harvesters are tabulated per volume and not weight. For the comparative harvesters in Ref. [21] (category 4) the mass of the fixed magnets is up to 48 g, which is much higher than the magnets in the dumbbell structure presented here, where the combined mass is 6 g. Also, the coils used in these comparative designs have up to 5600 turns, which is much higher than the 200 turns used in this study. These facts makes it hard to compare power and power density outright. A more logical metric is the power per unit mass, as this includes coils, tubing, magnets etc. As given in Table 1 the total mass of the harvester is 32.5 g and thus the maximum per unit mass is 32 μW/g. Compared to both Ref. [10] and Ref. [12], which is also targeted for human motion, the harvester produced here can potentially harvest three times as much power. In Table 2 we have listed the performance metrics of the harvester presented in this work, as well as that of comparable systems, where details on either the total mass or total volume of the system could be found. The conclusion is that the power density of the harvester reported in this study is high, given the small scale and small coils of the harvester. However, further research is needed to ascertain both fair and easily comparable harvester figure-of-merits for nearly all nonlinear harvester systems. In addition, further research could also consider optimizing the power production of the dumbbell harvester presented in this work. The latter can be done by considering the size of the coils, as well as the length of both the permanent magnets and the tube.

6. Conclusions

This paper described an electromagnetic energy harvester consisting of a free-to-move dumbbell structure with two magnets, two fixed magnets and two coils. The dumbbell structure has a number of benefits, namely increased magnetic flux change, potentially controllable resonance frequency and reduced friction.

The power of the harvester was characterized between 4 Hz and 20 Hz in steps of 0.5 Hz for a fixed amplitude of 3 mm. The harvester showed a softening resonator response with hysteresis between ascending and descending frequency sweeps. Furthermore, the harvester displayed two resonance peaks in power as function of drive frequency, with the peaks being of similar magnitude.

The maximum power produced by the harvester is 1.04 mW which occurs at 8.5 Hz in descending frequency sweep. Here the maximum acceleration of the harvester is 0.87 g. The power density of the harvester is 50 μ/cm^3 and the power per unit mass is 32 $\mu W/g$.

The voltage waveform as function of time for each drive frequency was analyzed by Fourier Transform to establish the main frequencies in the motion of the harvester. Here it was found that the two resonance peaks have different harmonics, with the first resonance peak characterized by higher order harmonics whereas the second resonance peak was primarily composed of response behavior at the excitation frequency.

CRediT authorship contribution statement

P. Holm: Investigation, Writing – original draft, Writing – review & editing, Methodology, Visualization. **C. Imbaquingo:** Conceptualization, Methodology, Writing – review & editing. **B.P. Mann:** Conceptualization, Writing – review & editing. **R. Bjørk:** Supervision, Writing – original draft, Writing – review & editing, Funding acquisition.

Data availability

All data presented in this manuscript, i.e. the voltage waveforms as function of time for all tested frequencies, are directly available from data.dtu.dk [43].

Acknowledgment

The authors wish to thank the Independent Research Fund Denmark, project 8022-00038B for sponsoring this work.

References

[1] I. Ahmad, L. Meng, A.M. Abdelrhman, S. Asad, M.S. Leong, Scopes, challenges and approaches of energy harvesting for wireless sensor nodes in machine condition monitoring systems : A review, Measurement 183 (2021) 109856.
[2] M.S. Ahmed, Designing of Internet of Things for real time system, Mater. Today: Proc. (ISSN: 2214-7853) (2021).
[3] D.J. Priya, S. Inman, Energy Harvesting Technologies, Springer, US, ISBN: 1281913359, 2009.
[4] B.P. Mann, N.D. Sims, Energy harvesting from the nonlinear oscillations of magnetic levitation, J. Sound Vib. 319 (1–2) (2009) 515–530.
[5] M. Gutierrez, A. Shahidi, D. Berdy, D. Peroulis, Design and characterization of a low frequency 2-dimensional magnetic levitation kinetic energy harvester, Sens. Act. A: Phys. 236 (2015) 1–10.
[6] C. Imbaquingo, C. Bahl, A.R. Insinga, R. Bjørk, A two-dimensional electromagnetic vibration energy harvester with variable stiffness, Appl. Energy 325 (2022) 119650.
[7] C.E.I. Munoz, C. Bahl, A.R. Insinga, R. Bjørk, Two-dimensional elliptically shaped electromagnetic vibration energy harvester, 2022, http://dx.doi.org/10.36227/techrxiv.20709031.v1, Techrxiv.
[8] C.R. Saha, T. O'donnell, N. Wang, P. McCloskey, Electromagnetic generator for harvesting energy from human motion, Sens. Act. A: Phys. 147 (1) (2008) 248–253.
[9] R. Morais, N.M. Silva, P.M. Santos, C.M. Frias, J.A.F. Ferreira, A.M. Ramos, J.A.O. Simoes, J.M.R. Baptista, M.C. Reis, Double permanent magnet vibration power generator for smart hip prosthesis, Sens. Act. A: Phys. 172 (1) (2008) 259–268.
[10] H. Liu, S. Gudla, F.A. Hassani, C.H. Heng, Y. Lian, C. Lee, Investigation of the nonlinear electromagnetic energy harvesters from hand shaking, IEEE Sens. J. 15 (4) (2014) 2356–2364.
[11] Q. Zhang, Y. Wang, E.S. Kim, Power generation from human body motion through magnet and coil arrays with magnetic spring, J. Appl. Phys. 115 (6) (2014) 064908.
[12] D.F. Berdy, D.J. Valentino, D. Peroulis, Kinetic energy harvesting from human walking and running using a magnetic levitation energy harvester, Sens. Act. A: Phys. 222 (2015) 262–271.
[13] M. Geisler, S. Boisseau, M. Perez, P. Gasnier, J. Willemin, I. Ait-Ali, S. Perraud, Human-motion energy harvester for autonomous body area sensors, Smart Mater. Struc. 26 (3) (2017) 035028.
[14] W. Wang, J. Cao, N. Zhang, J. Lin, W.-H. Liao, Magnetic-spring based energy harvesting from human motions: Design, modeling and experiments, Energy Conv. Manag. 132 (2017) 189–197.
[15] M.N. Struwig, R. Wolhuter, T. Niesler, Nonlinear model and optimization method for a single-axis linear-motion energy harvester for footstep excitation, Smart Mater. Struc. 27 (12) (2018) 125007.
[16] M. Masoumi, Y. Wang, Repulsive magnetic levitation-based ocean wave energy harvester with variable resonance: Modeling, simulation and experiment, J. Sound Vib. 381 (2016) 192–205.
[17] D. Castagnetti, A simply tunable electromagnetic pendulum energy harvester, Meccanica 54 (6) (2019) 749–760.
[18] N. Zhou, Y. Zhang, C.R. Bowen, J. Cao, A stacked electromagnetic energy harvester with frequency up-conversion for swing motion, Appl. Phys. Lett. 117 (16) (2020) 163904.
[19] D. Castagnetti, F. Dallari, Design and experimental assessment of an electromagnetic energy harvester based on slotted disc springs, Proc. Inst. Mech. Eng. Part L: J. Mater.: Des. Appl. 231 (1–2) (2017) 89–99.
[20] Y. Choi, S. Ju, S.H. Chae, S. Jun, C.-H. Ji, Low-frequency vibration energy harvester using a spherical permanent magnet with controlled mass distribution, Smart Mater. Struc. 24 (6) (2015) 065029.
[21] P. Carneiro, M.P. Soares dos Santos, A. Rodrigues, J.A.F. Ferreira, J.A.O. Simões, A.T. Marques, A.L. Kholkin, Electromagnetic energy harvesting using magnetic levitation architectures: A review, Appl. Energy 260 (2020) 114191.
[22] H.T. Nguyen, D.A. Genov, H. Bardaweel, Vibration energy harvesting using magnetic spring based nonlinear oscillators: Design strategies and insights, Appl. Energy 269 (2020) 115102.

[23] P.M.R. Carneiro, J.V. Vidal, P. Rolo, I. Peres, J.A.F. Ferreira, A.L. Kholkin, M.P. Soares dos Santos, Instrumented electromagnetic generator: Optimized performance by automatic self-adaptation of the generator structure, Mech. Syst. Signal Process 171 (2022) 108898.
[24] P. Constantinou, P.H. Mellor, P.D. Wilcox, A magnetically sprung generator for energy harvesting applications, IEEE/ASME Trans. Mech. 17 (3) (2012) 415–424.
[25] G. Aldawood, H.T. Nguyen, H. Bardaweel, High power density spring-assisted nonlinear electromagnetic vibration energy harvester for low base-accelerations, Appl. Energy 253 (2019) 113546.
[26] E. Dallago, M. Marchesi, G. Venchi, Analytical model of a vibrating electromagnetic harvester considering nonlinear effects, IEEE Trans. Power Elec. 25 (8) (2010) 1989–1997.
[27] A. Munaz, B.C. Lee, G.S. Chung, A study of an electromagnetic energy harvester using multi-pole magnet, Sens. Act. A: Phys. 201 (2013) 134–140.
[28] D.J. Apo, S. Priya, High power density levitation-induced vibration energy harvester, Energy Harv. Syst. 1 (1–2) (2014) 79–88.
[29] K. Kecik, Energy recovery from a non-linear electromagnetic system, Acta Mech. Auto. 12 (1) (2018).
[30] M.P. Soares Dos Santos, J.A.F. Ferreira, J.A.O. Simões, R. Pascoal, J. Torrão, X. Xue, E.P. Furlani, Magnetic levitation-based electromagnetic energy harvesting: A semi-analytical non-linear model for energy transduction, Sci. Rep. 6 (1) (2016) 1–9.
[31] C.M. Saravia, J.M. Ramírez, C.D. Gatti, A hybrid numerical-analytical approach for modeling levitation based vibration energy harvesters, Sens. Act. A: Phys. 257 (2017) 20–29.
[32] C. Imbaquingo, Energy Harvesting with Permanent Magnets (PhD dissertation), Technical University of Denmark, 2021.
[33] K. Pancharoen, D. Zhu, S.P. Beeby, Temperature dependence of a magnetically levitated electromagnetic vibration energy harvester, Sens. Act. A: Phys. 256 (2017) 1–11.
[34] T. Von Büren, P. Lukowicz, G. Tröster, Kinetic energy powered computing - An experimental feasibility study, Proc. Int. Symp. Wear. Comp. (2003) 22–25.
[35] A.E. Fitzgerald, C. Kingsley, S.D. Umans, Electric Machinery, McGraw-Hill, ISBN: 0071230106, 2003.
[36] W. Wang, H. Wei, Z.-H. Wei, Numerical analysis of a magnetic-spring-based piecewise nonlinear electromagnetic energy harvester, Euro. Phys. J. Plus 137 (1) (2022) 56.
[37] E. Blokhina, A. El Aroudi, E. Alarcon, D. Galayko, Nonlinearity in energy harvesting systems - Micro- and nanoscale applications, ISBN: 978-3-319-20355-3, 2016.
[38] K. Kecik, A. Mitura, S. Lenci, J. Warminski, Energy harvesting from a magnetic levitation system, Internat. J. Non-Linear Mech. 94 (2017) 200–206.
[39] T.W. Jensen, A.R. Insinga, J.C. Ehlers, R. Bjørk, The full phase space dynamics of a magnetically levitated electromagnetic vibration harvester, Sci. Rep. 11 (1) (2021) 16607.
[40] C. Imbaquingo, B. Mann, M. Beleggia, C. Bahl, R. Bjørk, Electromagnetic vibration energy harvester with ring magnets, Int. J. Acous. Vib. 26 (2) (2021) 1–9.
[41] C.E. Imbaquingo, M. Beleggia, A.R. Insinga, C.R.H. Bahl, B. Mann, R. Bjørk, Analytical force and flux for a 1-D electromagnetic vibration energy harvester, IEEE Trans. Magn. 56 (11) (2020) 1–6.
[42] A. Nammari, L. Caskey, J. Negrete, H. Bardaweel, Fabrication and characterization of non-resonant magneto-mechanical low-frequency vibration energy harvester, Mech. Syst. Sig. Proc. 102 (2018) 298–311.
[43] P. Holm, C. Imbaquingo, R. Bjørk, Data set for high power electromagnetic vibration harvesting using a magnetic dumbbell structure, data.dtu.dk, 2022, http://dx.doi.org/10.11583/DTU.21302874.